Elastic Break-Up of 156 MeV ^{6}Li Projectiles With Large Asymptotic Relative Momenta of the Fragments

N. Heide, H. Rebel, V. Corcalciuc, H. J. Gils, H. Jelitto,
J. Kiener, J. Wentz, S. Zagromski, D. K. Srivastava
Institut für Kernphysik

Kernforschungszentrum Karlsruhe

KERNFORSCHUNGSZENTRUM KARLSRUHE

Institut für Kernphysik

KfK 4564

Elastic Break-Up of 156 MeV 6Li Projectiles With Large Asymptotic Relative Momenta of the Fragments

N. Heide, H. Rebel, V. Corcalciuc*, H.J. Gils, H. Jelitto,
J. Kiener, J. Wentz, S. Zagromski and D.K. Srivastava**

*   Central Institute of Physics, IFIN, Bucharest, Romania
**   Bhabha Atomic Research Centre, V.E.C.C., Calcutta, India

Abstract

The triple differential cross sections for elastic break-up of 156 MeV ^{6}Li projectiles by the reactions ^{208}Pb (^{6}Li, ad) ^{208}Pb$_{g.s.}$ and ^{12}C (^{6}Li, ad) ^{12}C$_{g.s.}$ have been measured with large asymptotic relative momenta of the outgoing fragments. The data exhibit rather unfamiliar shapes of the energy spectra, often replacing the usual bell-shape distributions by double-peaked structures and varying rapidly with the relative emission angles. The origin of these features has been explored and the cross sections have been analysed on the basis of a diffractive disintegration approach.

ELASTISCHER AUFBRUCH VON 156 MEV ^{6}Li PROJEKTILEN MIT GROSSEN ASYMPTOTISCHEN RELATIVIMPULSEN DER FRAGMENTE

Die dreifach differentiellen Wirkungsquerschnitte für den elastischen Aufbruch von 156 MeV ^{6}Li Projektilen in den Reaktionen ^{208}Pb (^{6}Li, ad) ^{208}Pb$_{g.s.}$ und ^{12}C (^{6}Li, ad) ^{12}C$_{g.s.}$ wurden bei großen asymptotischen Relativimpulsen der Fragmente gemessen. Die experimentellen Daten zeigen ungewöhnliche Energiespektren der Fragmente wobei oft die übliche glockenförmige Verteilung durch Doppelpeak-Strukturen ersetzt wird, die rasch mit dem Relativwinkel variieren. Die Herkunft dieses Verhaltens der Wirkungsquerschnitte wird im Rahmen eines diffraktiven Aufbruchmodells erforscht.

CONTENT

1. INTRODUCTION

There are many different reaction types which produce projectile-like fragments in collisions of light and heavy ions. Basically they evolve from two extreme scenarios: (i) after inelastic scattering or picking-up a few nucleons from the target, the projectile is excited into a resonance state of the continuum and decays subsequently ("sequential break-up"), or alternatively (ii) a loosely bound substructure of the projectile ("participant") interacts with the target whereas the "spectator" part misses it and is immediately lifted into the continuum ("direct break-up"). In the latter case, the spectator is assumed to continue its journey almost unperturbed, with approximately the beam-velocity superimposed by the Fermi-motion of the spectator-cluster inside the projectile. The participant cluster is either elastically scattered or undergoes any kind of nonelastic interactions. In view of such a spectator-participant picture of the process

$$a (= b + c) + A \rightarrow b + (c + A)^* ,$$ (1.1)
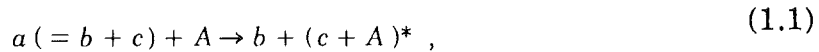
originally formulated by Serber [1] in a geometrical model, the quasi free transition amplitude (involving the plane-wave approximation)

$$T_{if} = T_{cA} (\mathbf{Q}) \cdot \tilde{\phi} (q)$$ (1.2)

can be expressed [2] in terms of the internal momentum distribution $| \tilde{\phi}_{bc} (q) |^2$ with $q = k_b - m_b/m_a k_i$ and of the half-off-shell scattering amplitude $T_{cA} (\mathbf{Q})$ of the participant-target interaction inducing the break-up and being dependent on the momentum transfer $\mathbf{Q} = k_i - k_f$.

In detailing this view on direct break-up the question arises in which way the experimental cross sections really reflect the structure of the amplitudes $T_{cA} (\mathbf{Q})$ and $\tilde{\phi} (q)$, and which distortions significantly affect the primary features, thus obscuring experimental information on these quantities. Faced with the large complexity of fragmentation processes, the elastic break-up mode

$$a (= b + c) + A \rightarrow b + c + A_{g.s.} ,$$ (1.3)
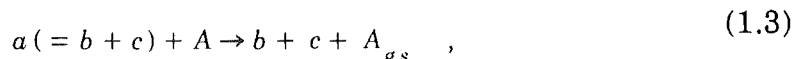
otherwise called [3] *"free dissociation"* in the nuclear field, is expected to provide the most transparent situation for exploring such aspects.

This paper reports on investigations of the elastic break-up of 156 MeV ^{6}Li projectiles by measuring the triple differential cross sections $d^3\sigma/ (d\Omega_\alpha \, d\Omega_d \, dE_\alpha)$ for the reactions ^{208}Pb $(^6$Li, α d $)$ ^{208}Pb$_{g.s.}$ and ^{12}C $(^6$Li, α d $)$ ^{12}C$_{g.s.}$. The case of ^{6}Li is of particular interest since ^{6}Li induced reactions reveal generally a transitional behaviour [4] between features observed in light and heavy ion reactions. Due to the pronounced α - d cluster structure the enhanced probability for breaking-up into two distinctly different fragments is of advantage when identifying various

reaction paths. The present experiments isolate the elastic break-up mode via kinematically complete measurements. Unlike most of other studies of light projectile break-up, the detectors measuring the energy spectra observe the coincident fragment emission under relatively large emission angles. In this way the contributions of smaller relative momenta (including sequential break-up through low-lying resonance states) are largely excluded, and usually obscured features associated with large momenta and small coincident cross sections, are brought to the fore. In fact, the measurements reveal rather unfamiliar shapes of energy spectra of break-up fragments rapidly varying with the relative emission angle and dissolving the bell-shaped bumps of the cross sections in conspicuous double-peaked structures. This phenomenon may arise from a coherent cooperation of the specific shape of the Fermi-momentum distribution and of the fragment-target interactions in the considered range of momentum transfer and relative momenta [5]. Additionally, through exchange of the roles of the spectator and the "elastically" scattered participant two different amplitudes appear and interfere.

The data are analysed on the basis of the diffractive dissociation approach [6,7] of exclusive light ion disintegration processes, expressing the break-up amplitudes in terms of parametrized profile functions of the clusters interacting with the target nucleus. Though this approach implies some questionable simplifications, the analysis gives an qualitative account and indicates significantly the influence of second-order processes with both fragments being (off-shell) scattered ("double-scattering").

2. EXPERIMENT

The measurements of the triple differential cross secions $d^3\sigma/(d\Omega^L_\alpha \, d\Omega^L_d \, dE^L_\alpha)$ for the $^6Li \rightarrow \alpha + d$ break-up in the field of ^{12}C and ^{208}Pb used the analyzed beam facilities of the Karlsruhe Isochronous Cyclotron. $^6Li^{3+}$ ions, produced by the external ECR-source LISKA [8] were accelerated to 156 MeV and focussed within a 1.5 mm Ø spot onto the targets: ^{208}Pb (4 mg/cm2, enr. 98.2%) and ^{12}C (4.2 mg/cm2, nat. enr.) respectively. The energy spread of the analyzed beam was about 120 keV (FWHM) and the average beam current about 3 nA. A well shielded Faraday cup placed ca. 2 m behind the exit of the 135 cm Ø target chamber stopped the beam and the accumulated charge was measured by a usual current digitizer. The 33 MHz cyclotron was operated in the so called 3 : 1 mode, so that the time distance between two beam pulses was ca. 90 ns.

2.1. POSITION SENSITIVE CHARGED–PARTICLE DETECTION

The outgoing charged reaction products, in particular α-particles and deuterons, have been detected by two semiconductor telescopes, each consisting of a 500 μm thick position sensitive, totally depleted ion implanted Silicon ΔE - detector and a 21 mm thick high purity intrinsic Germanium E-detector in which the high energy deuterons also could be stopped. Together with the liquid-nitrogen cooling systems both detectors were positioned on two movable arms inside the scattering chamber. The operational temperature of the E-detectors was about 77 K. Tab. 1 lists some properties of the detector set-up. The acceptance of the telescopes has been defined by 8 mm thick tantalum diaphragms. For each telescope the total angular acceptance covers 3.3° (corresponding to a solid angle of 304.7 μsr) which could be electronically subdivided in smaller angular bins via position sensitive detection of the fragments.

Tab. 1   Some characteristics of the detector set-up.

ΔE-Si-detectors	Telescope I	Telescope II
Active area	15 x 8 mm^2	15 x 8 mm^2
Active thickness	485 μm	485 μm
Energy resolution (5.47 MeV α-particles)	< 30 keV (FWHM)	< 30 keV (FWHM)
Position resolution	<0.15 mm	< 0.15 mm

E-Ge-detectors		
Active area	200 mm^2	200mm^2
Active thickness	21 mm	21 mm
Energy resolution (5.47 MeV α-particles)	< 22 keV (FWHM)	< 20 keV (FWHM)
Energy resolution (104 MeV α-particles analysed beam)	< 180 keV (FWHM)	< 160 keV (FWHM)

The energy calibration is based on elastic scattering of protons, deuterons, α-particles and [6]Li-ions at 26 MeV/N. Fig. 1 displays typical 2-dimensional ΔE-E spectra, showing the separation of different charged particles in different electronic channels. When constructing the energy spectra particle identification is done off-line by setting adequate windows. Fig. 2 shows a position spectrum for elastically scattered α-particles where the full angular acceptance (3.3°) is
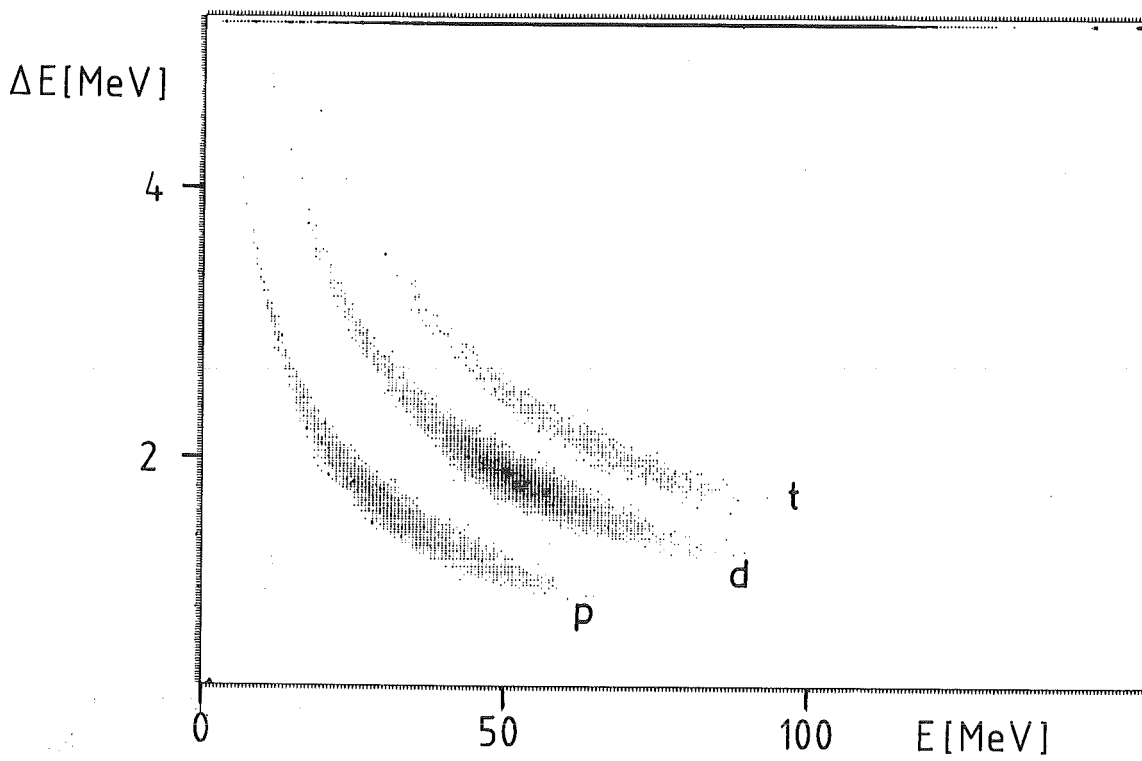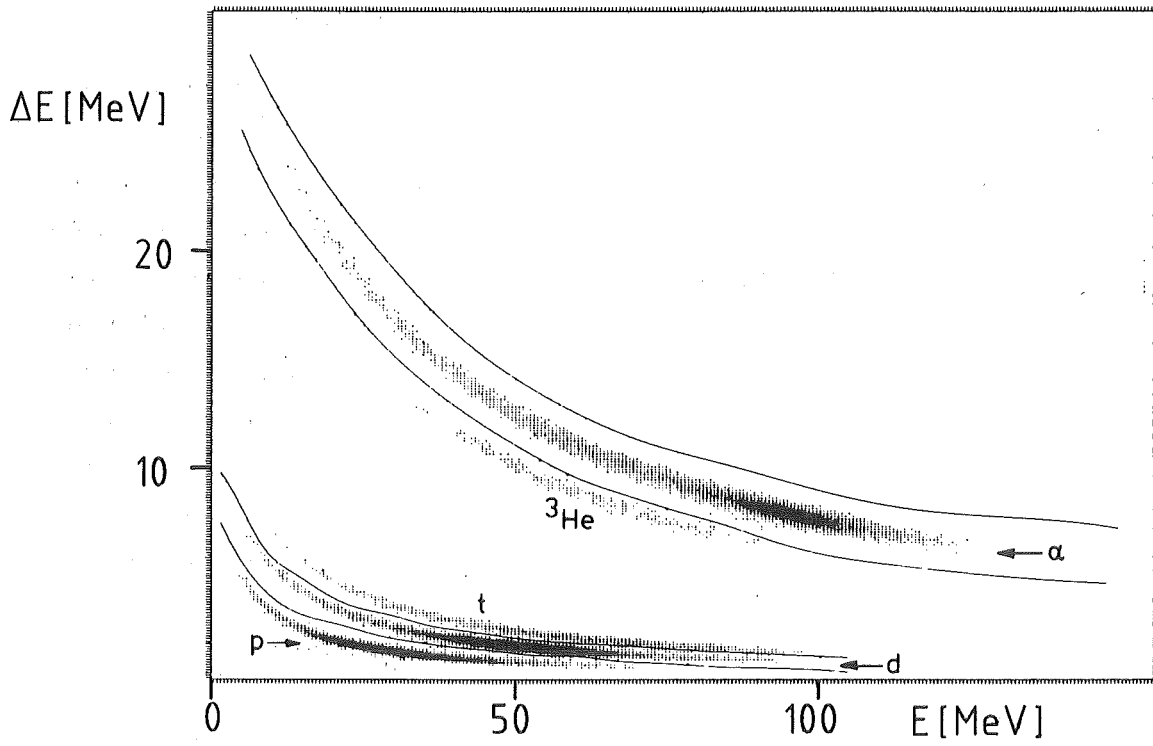
Fig. 1   ΔE-E particle identification spectra in two different electronic channels.
The spectrum of Li particles is electronically suppressed.

subdivided into six bins of the width of 0.55°. The linearity of the position determination has been checked by positioning proper mechanical slits ("comb"). Nonlinearities arise at high counting rates for particles with small energy losses in the ΔE detector, i.e. for protons. The effect is of minor importance for deuterons and negligible for α-particles. Including uncertainties due to the finite vertical acceptance and beam spot size the uncertainties of relative emission angle determination are estimated to be $\pm$ 0.06° for α-particles and $\pm$ 0.09° for deuterons. The absolute zero of the angular scale is checked by observing the distinct diffraction pattern of elastic scattering. More details of the operational procedures of the detector system are given in Ref. 9.
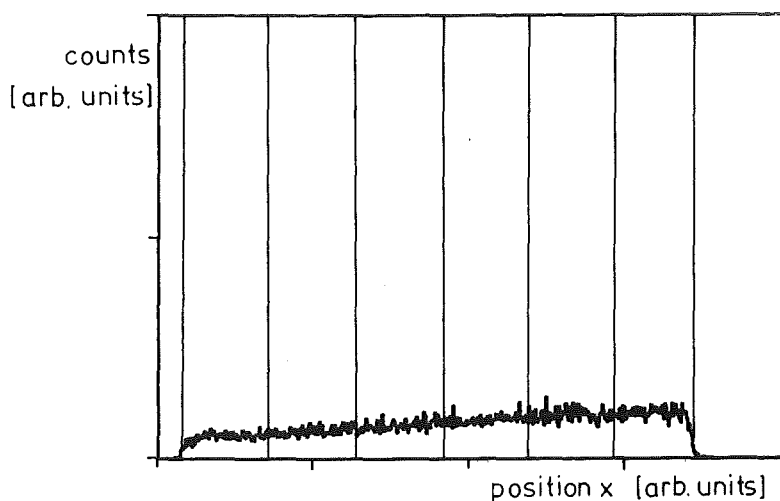
Fig. 2   Position spectrum of scattered α-particles divided in 6 bins, each corresponding to a width of 0.55° of the angular acceptance in the present detector set-up.

2.2. ELECTRONICS

Each one of the two telescopes generates three analog signals : E_T proportional to the energy loss ΔE, E_x proportional to the horizontal position X and to ΔE, and the rest-energy signal E. From E_T and E_x a signal $E_x / E_T \propto X$ is deduced by the data acquisition computer, defining finally the emission angle of the detected fragment.

The electronic scheme (Fig. 3) is basically a fast - slow coincidence circuit. There are two (slow) ΔE analog channels for each telescope, differing in the amplification in order to allow particle identification of the less ionising hydrogen isotopes with the same quality as for larger-Z particles. The fast logic circuit

ATT Attenuator
CD   Cable delay
CFD Constant fraction discriminator
CU   Coincidence unit
D   Discriminator
DA   Delay amplifier
DLA Delay line amplifier
FD   Frequency divider
GDG Gate and delay generator
INV Inverter
LG   Linear gate
LGS Linear gate & stretcher
PA   Preamplifier
SA   Spectroscopy amplifier
TFA Timing filter amplifier
TPC Time to pulse height converter
UC   Universal coincidence

Fig. 3 Diagram of the electronic set-up

checks first the coincidence of corresponding E_T and E signals. A veto signal generated in each telesope branch allows the suppression of a certain window of the ΔE - E spectra, in particular of elastically scattered 6Li which would otherwise induce random coincidences and pile-up effects. The ΔE - E coincidence units generate the start- and stop-signals, respectively, for the time - to pulse - height - converter (TPC). True coincidences are characterized by a fixed time relation between the fast signals of the two channels ("prompt peak"), which is selected by a proper window in the off-line processing of the data.

The ΔE - E coincidence units generate additionally frequency divided logic signals feeding a universal coincidence unit together with the TPC output signal. The universal coincidence acts as a logic "OR" device, so that each of these input signals are able to open the linear gates (LG) of the analog branches. This scheme admits not only processing of coincidence events but also the frequency-divided registration of single events of each telescopes. The output signals of the ADC's
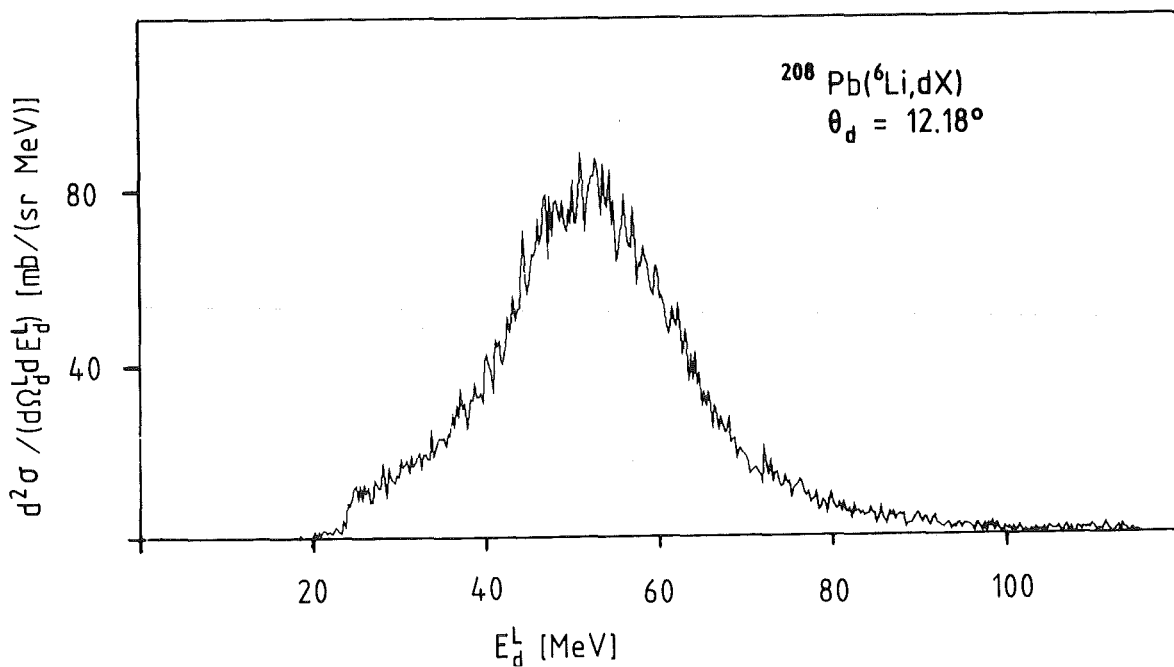
Fig. 4   Singles spectrum of deuterons emitted with a reaction angle $\theta = 12.18°$ from collisions of 156 MeV 6Li with 208Pb.

are written on magnetic tape in list mode by a PDP 11 computer and afterwards processed by off-line sorting programs.

Fig. 4 shows as an example a singles spectrum of deuteron ejectiles from collisions of 156 MeV ^{6}Li with ^{208}Pb.

2.3. IDENTIFICATION OF DIRECT ELASTIC BREAK-UP

Due to the kinematic constraints when observing three outgoing particles, for each particular Q-value the laboratory energies E_d and E_α of the two projectile fragments are correlated on a well defined kinematical locus in the $E_d - E_\alpha$ plane. Actually due to the small recoil energy of the target nucleus the (binary) break-up locus is well approximated by a linear relation

$$E_d^{Lab} + E_\alpha^{Lab} = E_{Li}^{Lab} - Q_3 - E_{ex} \qquad (2.1)$$

even for the ^{12}C target in our case, where $Q_3 = 1.47$ MeV and E_{ex} is the excitation energy of the nucleus. Fig. 5 gives a Q_3 spectrum summed over an angular range of 3.3° for the case of ^{12}C (^{6}Li, αd) ^{12}C ($\theta_\alpha = 14°$, $\theta_d = -14°$) showing the elastic ($E_{ex} = 0$ MeV) and inelastic ($E_{ex} = 4.4$ MeV) break-up, resulting from summing up the events populating the corresponding kinematic loci. A typical scatter-plot of elastic break-up events of ^{208}Pb (^{6}Li, αd) ^{208}Pb$_{g.s.}$ is shown in Fig. 6. Fig. 7 displays the dependence of the relative energy of the α- and d-fragments vs the laboratory α-particle-energy, indicating the so called "magnifying glass" effect - a remarkably slow variation of $E_{\alpha d}$ vs the laboratory energies of the coincidently emitted fragments. The minimum value of $E_{\alpha d}$, taken near the beam-velocity energies is determined by the relative emission angles $\theta_{\alpha d}$. With our set-up using larger relative emission angles, smaller relative energies, including the resonances at $E_{\alpha d} = 0.71$ MeV (3_1^+ state at 2.18 MeV) and $E_{\alpha d} = 2.84$ MeV (2^+ state at 4.31 MeV) e.g. are cut off, thus selecting direct break-up events with larger relative energies (> 5 MeV).

3. MEASURED COINCIDENCE CROSS SECTIONS

All measurements were done in an in-plane - geometry with the detectors positioned at different sides of the incoming ^{6}Li beam (indicated by different signs of the emission angles). The angular range studied for elastic α - d - break-up of 156 MeV ^{6}Li on ^{208}Pb and ^{12}C, respectively covers 14.88° to 12.18° for one telescope (I) and -16.88° to -12.88° for the other telescope (II). Typical coincidence spectra are displayed in Figs. 8 - 10. The width of the energy bins is 2 MeV. The error bars of the cross sections represent the statistical error, while the uncertainty in the absolute scale is estimated to be less than 25%. A compilation of all
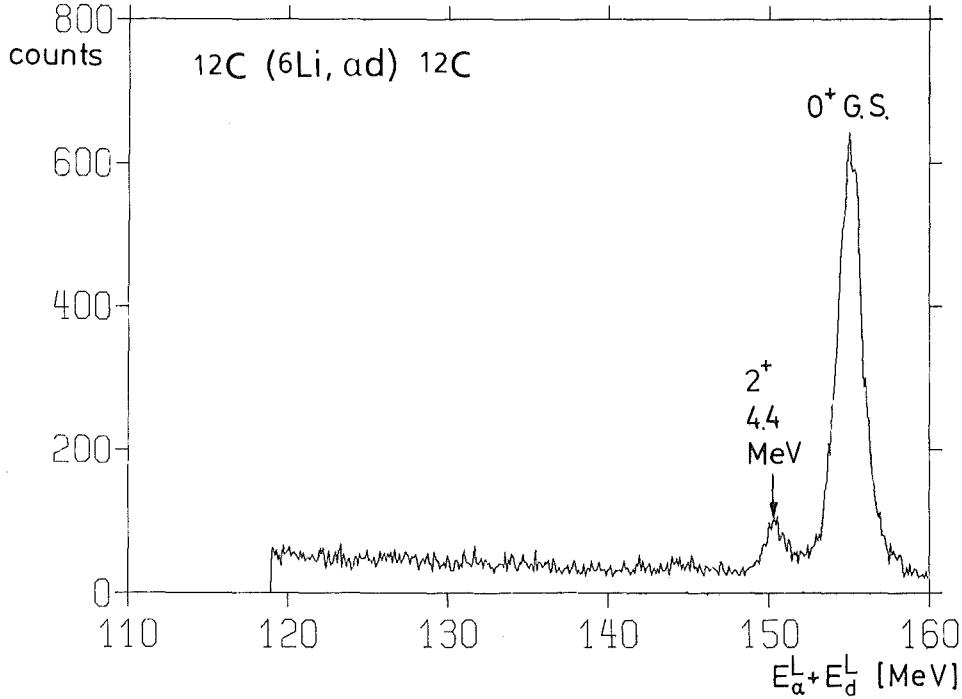
Fig. 5 Q_3-value spectrum from the reaction ^{12}C (^6Li, αd) ^{12}C at E_{Li} = 156 MeV.

the measured coincidence spectra, together with tables of numerical values is given in Ref. 10. The corresponding angular correlations $d^2\sigma / (d\Omega^L_\alpha \, d\Omega^L_d)$ (given in Ref. 11) are not very exclusive since they cover only a small angular range.

The data for smaller relative emission angles (Fig. 11) show the typical beam-velocity bell-shaped break-up bump, which may be basically understood as originating from the spectator-participant picture. The post-form DWBA theory worked out by Baur et al [12] is able to describe this cross section on absolute scale. However, the double-peaked structure (less pronounced and due to larger statistical errors less significant in the ^{12}C case) which evolves at larger relative emission angles (Figs. 8 - 10) is expected to result from delicate interferences, explicitely affected by the shape of the momentum distribution $| \tilde{\phi} \, (q) |^2$. Thus, the zero-range post-form DWBA appears to be not adequate for the analysis. In the present paper the data are analysed using a more phenomenological approach based on a diffractive disintegration model worked out by Sitenko et al [6,7].
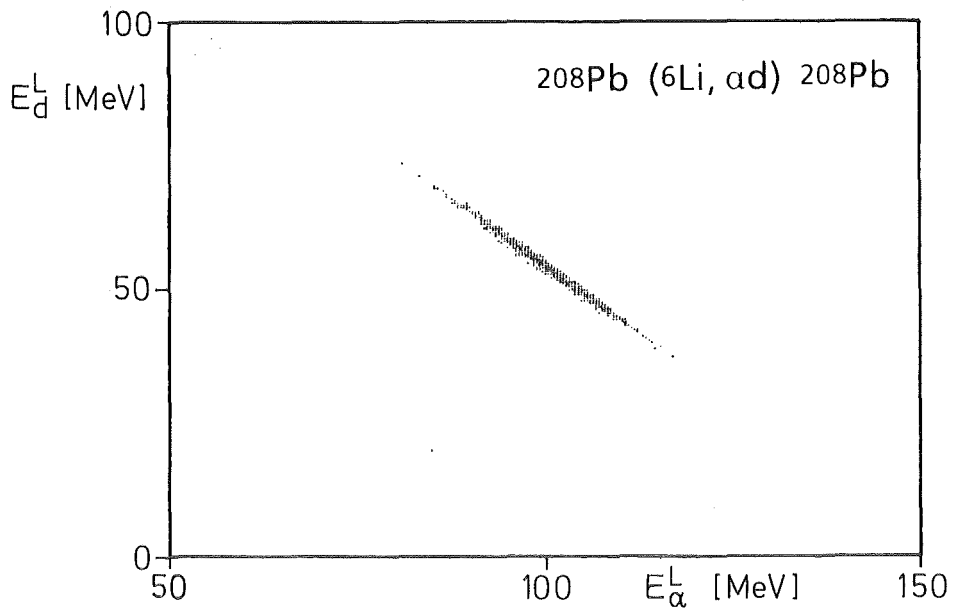
Fig. 6 E_d^L - E_α^L scatter plot for the reaction 208Pb (6Li, ad) 208Pb. The coincidence events populate the kinematical locus for the elastic break-up.
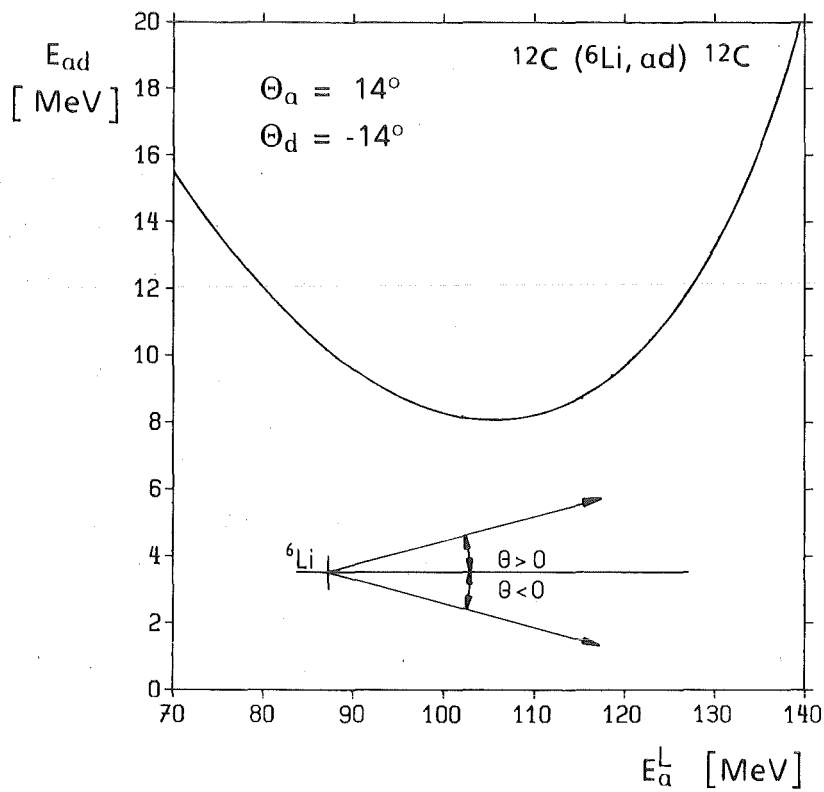
Fig. 7   Relative energy dependence of the break-up fragments from the 12C (6Li, ad) 12C reaction at 156 MeV versus the laboratory a-particle energy.
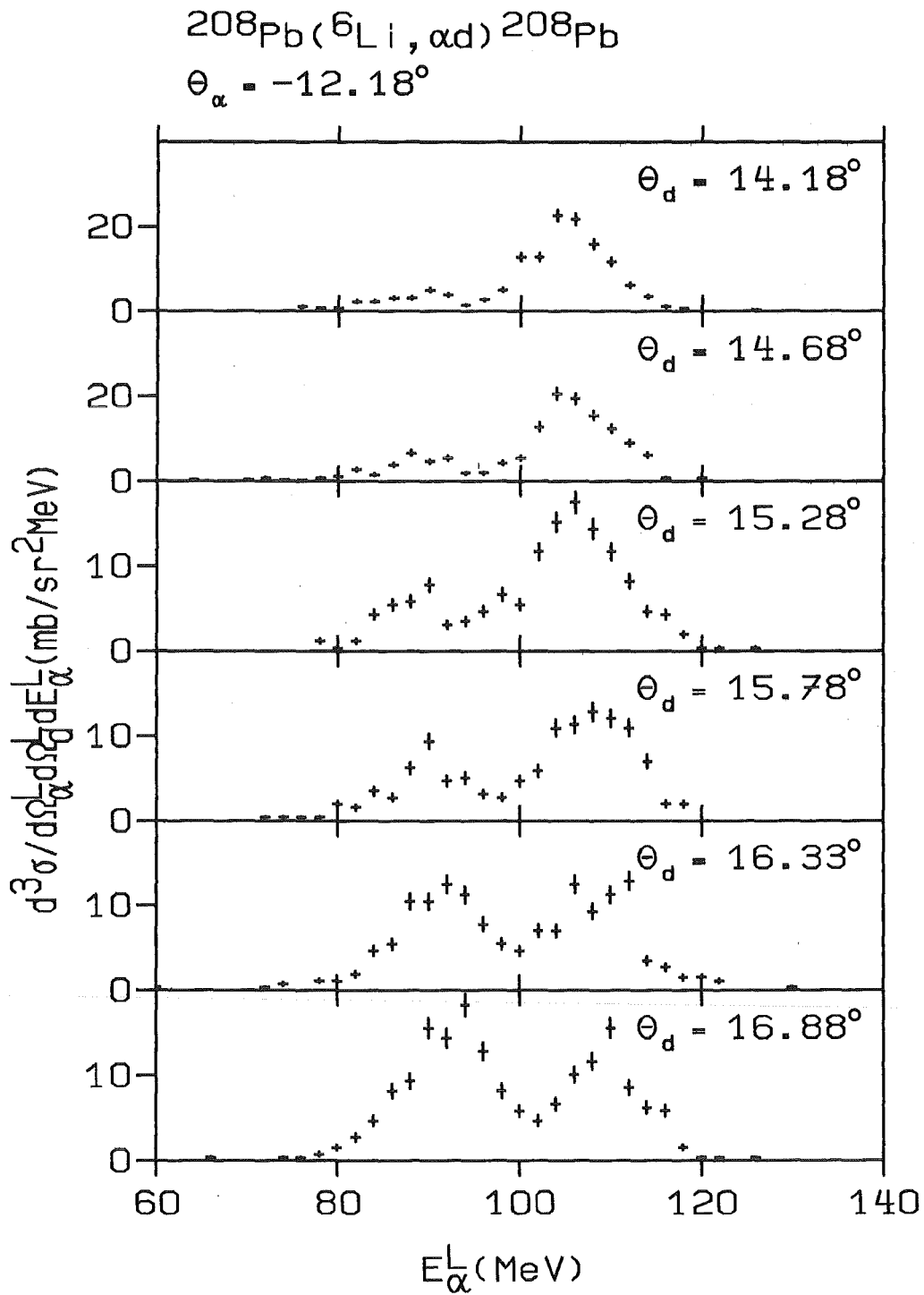
Fig. 8   Coincidence cross sections for the 208Pb (6Li, αd) 208Pb$_{g.s.}$ reaction at E$_{Li}$ = 156 MeV (laboratory angles θ$_α$ fixed, θ$_d$ varying).

$$^{208}Pb(^6Li, \alpha d)^{208}Pb$$

$$\Theta_d = -14.88°$$
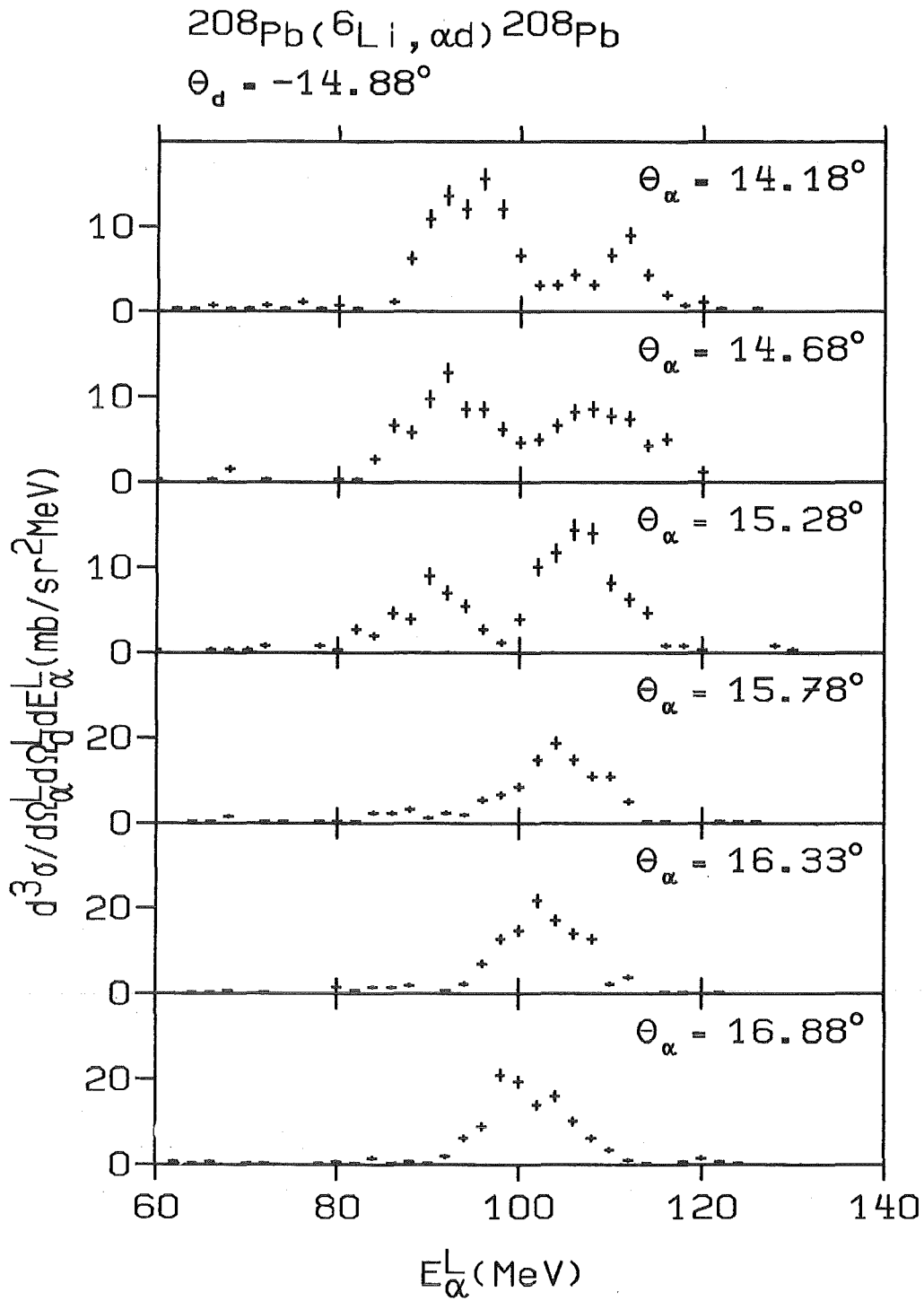
Fig. 9   Coincidence cross sections for the ^{208}Pb (^{6}Li, αd) ^{208}Pb$_{g.s.}$ reaction at $E_{Li} = 156$ MeV (laboratory angles θ_d fixed, θ_α varying).
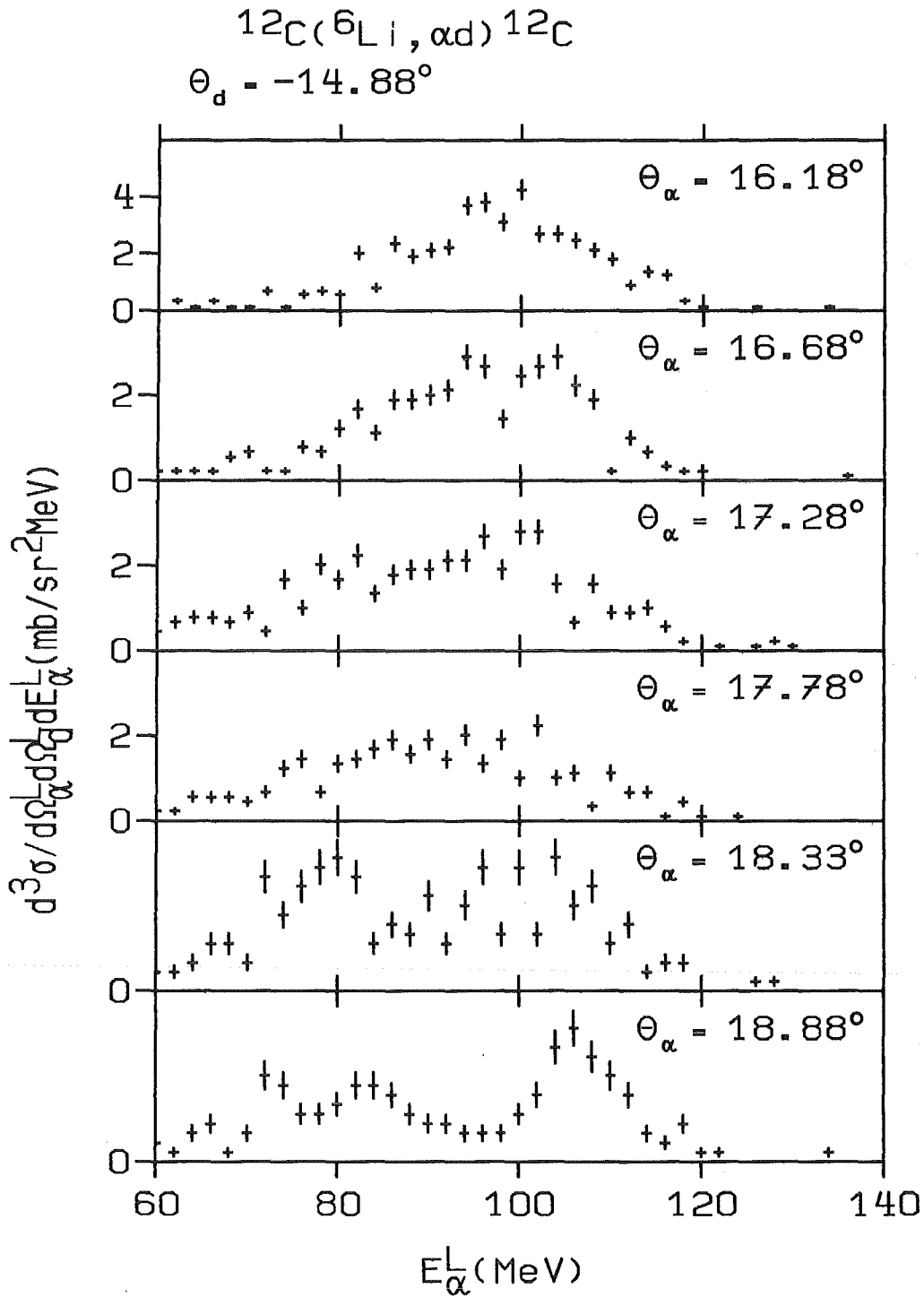
Fig. 10   Coincidence cross sections for the ^{12}C (^{6}Li, αd) ^{12}C$_{g.s.}$ reaction at $E_{Li} = 156$ MeV.
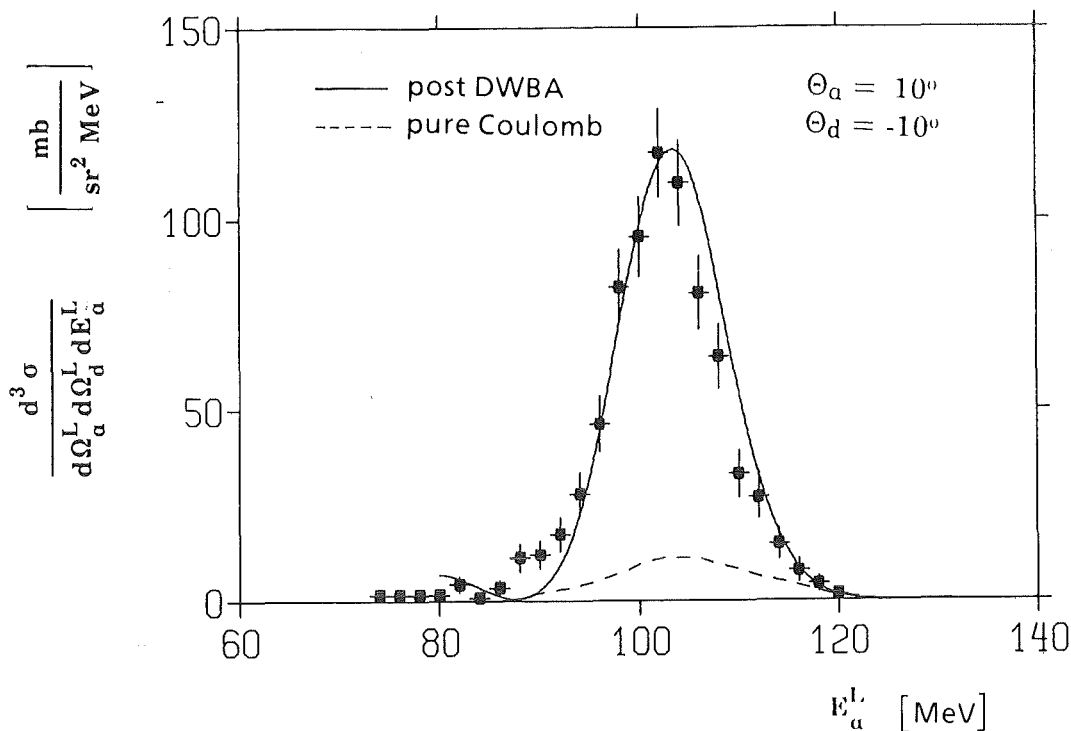
Fig. 11   Measured coincident cross section d3σ / (dΩ$_α$^{L} dΩ$_d$^{L} dE$_α$^{L}) of the elastic break-up of 156 MeV ^{6}Li projectiles on ^{208}Pb as compared with the post-form DWBA prediction (using the value D$_0$ = 0.53·10^4 MeV^2 fm^3 for the zero range constant).

4.   DIFFRACTIVE DISSOCIATION APPROACH
4.1   FORMALISM

An appealing feature of the diffractive dissociation treatment worked out by Sitenko et al. [6,7] is the transparent manner in which the half-off-shell T-matrix for the scattering of the incoming projectile enters.

With the explicit use of the eikonal approximation the amplitude for elastic break-up

$$a + A \rightarrow b + c + A_{g.s.} \tag{4.1}$$

is given by

$$f^{bu}(\mathbf{Q}, \mathbf{k}) = \frac{ik_i}{2\pi} \int d\mathbf{b}\, e^{i\mathbf{Q}\cdot\mathbf{b}} \int d\mathbf{r}\, \phi_k^{(-)*}(\mathbf{r})\, \omega(\mathbf{b})\, \phi_a(\mathbf{r}) \tag{4.2}$$

where k$_i$ is the momentum of the projectile, $\mathbf{Q}$ is the momentum transfer and $\mathbf{k}$ is the relative momentum of the outgoing fragments.

$$Q = k_i - k_f \tag{4.3a}$$

$$k = (m_c/m_a)k_b - (m_b/m_a)k_c \tag{4.3b}$$

$$k_f = k_b + k_c \tag{4.3c}$$

The wave function ϕ_a describes the ground state of the projectile excited to the continuum represented by ϕ_k. The total profile function

$$\omega(b) = \omega_b(b_b) + \omega_c(b_c) - \omega_b(b_b) \cdot \omega_c(b_c) \tag{4.4}$$

is composed of the profile function of fragments (j)

$$\omega_j(b_j) = \frac{1}{2\pi i k_i} \int dQ\, e^{iQ \cdot b_j} f_j(Q) . \tag{4.5}$$

The impact vectors b_j are related by

$$b = \frac{m_b}{m_a} b_b + \frac{m_c}{m_a} b_c . \tag{4.6}$$

Using these notations we write the amplitude for the diffractive dissociation

$$f^{bu}(Q, k) = F\left(-\frac{m_c}{m_a} Q, k\right) f_b(Q) + F\left(+\frac{m_b}{m_a} Q, k\right) f_c(Q)$$

$$+ \frac{i}{2\pi k_i} \int dQ' F(Q', k) f_b\left(\frac{m_b}{m_a} Q - Q'\right) f_c\left(\frac{m_x}{m_a} Q + Q'\right) \tag{4.7}$$

where the inelastic form factor $F(Q, k)$ is defined by

$$F(Q, k) = \int dr\, \phi_k^{(-)*}(r)\, e^{iQ \cdot r} \phi_a(r) \tag{4.8}$$

and $f_j(Q)$ is the inverse of ω_j (eq. 4.5).

Assuming for the moment that double scattering of the clusters, given by the last term in eq. (4.7), is negligible and with the approximation[6,7]

$$\omega_b(b) = \omega_c(b) = \omega(b) \tag{4.9}$$

we get

$$\frac{d^3\sigma}{d\Omega_b\, d\Omega_c\, dE_b} \simeq \frac{\mu_{bx}}{(2\pi)^3} \frac{k_b k_c}{k_i} \left| \left[F\left(-\frac{m_c}{m_a} Q, k\right) + F\left(\frac{m_b}{m_a} Q, k\right) \right] f(Q) \right|^2 . \tag{4.10}$$

Thus, we notice that the triple differential cross-section is directly related to the *off-shell* scattering amplitude $f(Q)$ for the projectile-target interaction since, in

general $|k_f| < |k_i|$ due to the Q_3-value of the reaction and due to a non - zero value of the relative energy of the fragments. For the application to the measured ^{6}Li break-up data we use as a first approximation the 1S (Yukawa-type) ^{6}Li wave function

$$\phi_\alpha(r) = \sqrt{\frac{\alpha}{2\pi}}\ \frac{e^{-\alpha r}}{r} \tag{4.11}$$

and the scattering function

$$\phi_k(r) = e^{i\,k\,r} + \frac{1}{ik - \alpha}\ \frac{e^{-i\,k\,r}}{r} \tag{4.12}$$

where

$$\alpha = \sqrt{\frac{2\mu_{\alpha d}\cdot\varepsilon}{\hbar^2}} \tag{4.13}$$

with ε ($= 1.47$ MeV) the binding energy and $\mu_{\alpha d}$ the reduced mass.

Actually the Yukawa-type wave function (eq. 4.11) does not represent the large momentum components of the realistic [13] α - d wave function of ^{6}Li. But the analytic form of eq. 4.11 allows to calculate the inelastic form factor (eq. 4.8) analytically, and modifying the value of α or ε, respectively would simulate [14] a larger part of the realistic wave function.

4.2 ANALYSES

Differently from the procedure adopted in Ref. 15 where the vast amount of measured coincidence data has been considered in a plot of $d^3\sigma / (d\Omega_\alpha\, d\Omega_d\, dE_\alpha)^{exp}$ $/ | F (Q, k) |^2$ by use of an adequate form factor $F (Q)$, we analyse here the cross sections by introducing calculated scattering amplitudes $f(Q)$.

As long as the Coulomb break-up is assumed to be negligible for events with larger relative energies of the fragments, the scattering amplitude is the *nuclear* amplitude corrected for the Coulomb scattering effect. Different procedures may be used to approximate the half-on-shell amplitude $f(Q)$

(i) in the spirit of refs. 6 and 7 where a Fermi shape parametrization of the profile function (eq. 4.9) is proposed, we may more simply adopt the scattering amplitude for a "black disc" nucleus

$$f_N^{BL}(Q) = i\ k_i R_{BL}\cdot J_1(Q\cdot R_{BL})/Q \tag{4.14}$$

Approximating the Coulomb effect by a single phase $e^{i\sigma}$ (R_{BL}) does not affect the cross section.

(ii) alternatively $f(Q)$ can be derived from an optical model potential[17] describing the scattering of the projectile.

Fig. 12 displays the squared amplitudes: f_N^{BL} (R_{BL} = 10.2 fm) and f_N^{OP} (Q) for the case of 6Li + 208Pb scatttering. For the present experimental data the region around the minimum near Q = 0.35 fm^{-1} is relevant. Though the two amplitudes are rather similar there, small differences in magnitude and slope affect distinctly the triple differential cross sections. This is evident when inspecting figs. 13 and 14 which compare some representative experimental results with theoretical predictions based on different forms of the scattering amplitude.
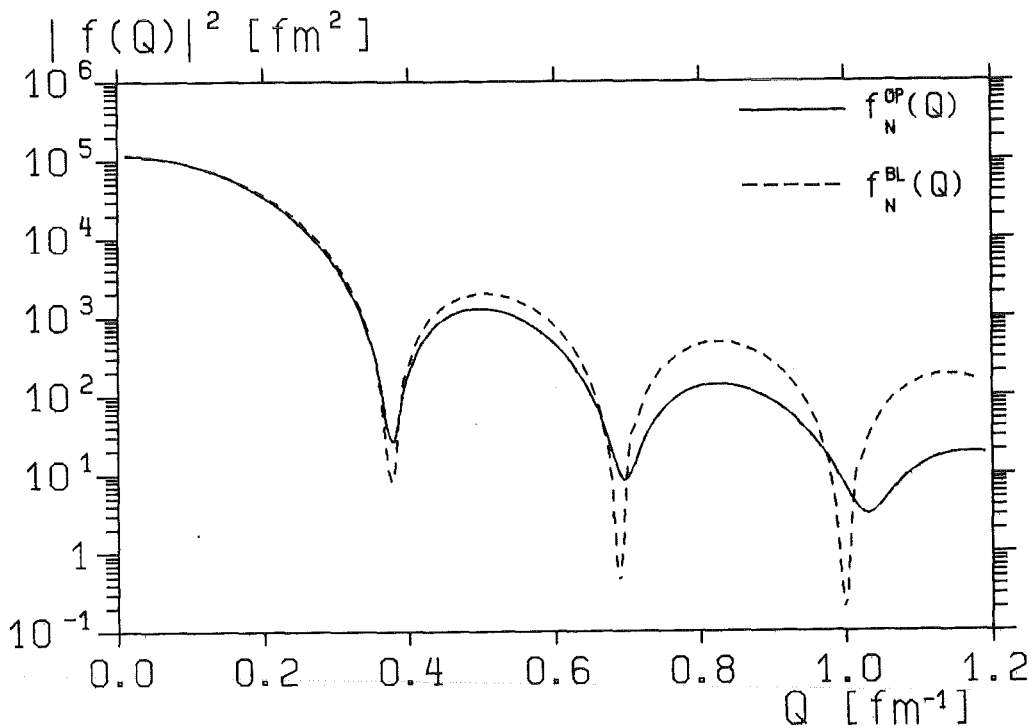
Fig. 12   Two forms of the squared scattering amplitude describing the
        6Li + 208Pb *nuclear* scattering.

The theoretical cross sections are normalized by using the prevailing value [13] of the spectroscopic factor C^2S = 0.7.
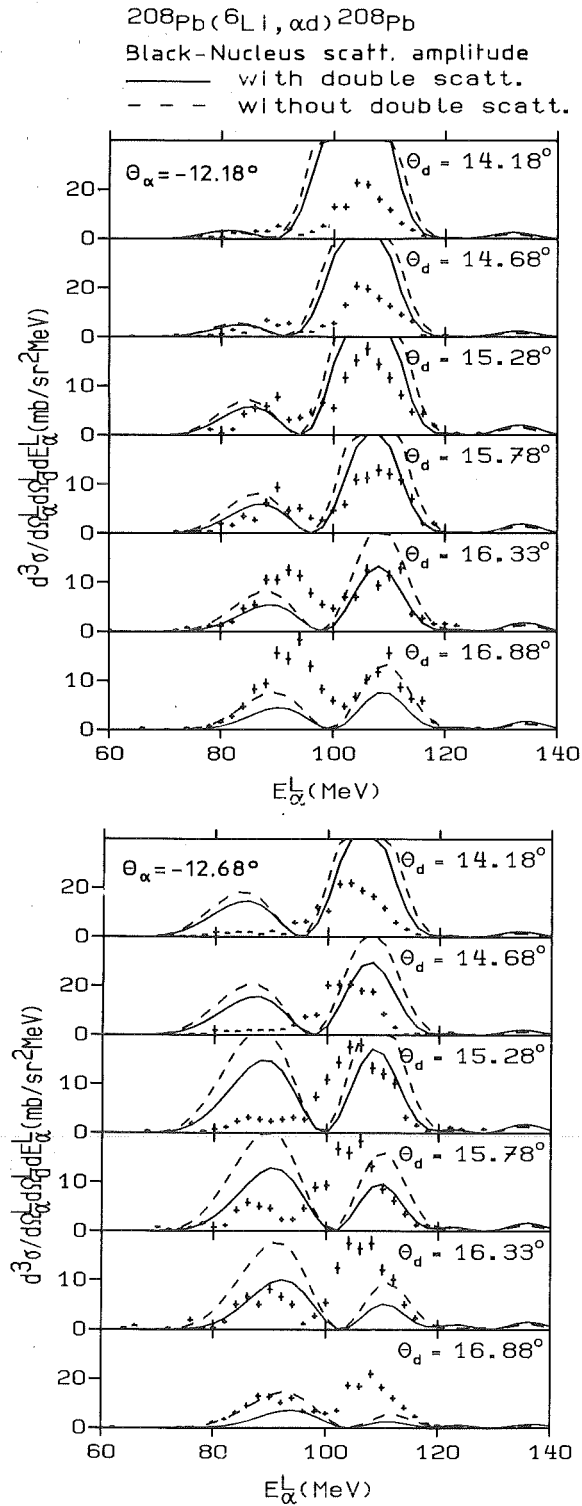
Fig. 13 Experimental and theoretical triple differential cross sections of elastic break-up of 156 MeV ^{6}Li projectiles colliding with ^{208}Pb: The theoretical description uses the "black-nucleus" scattering amplitude.
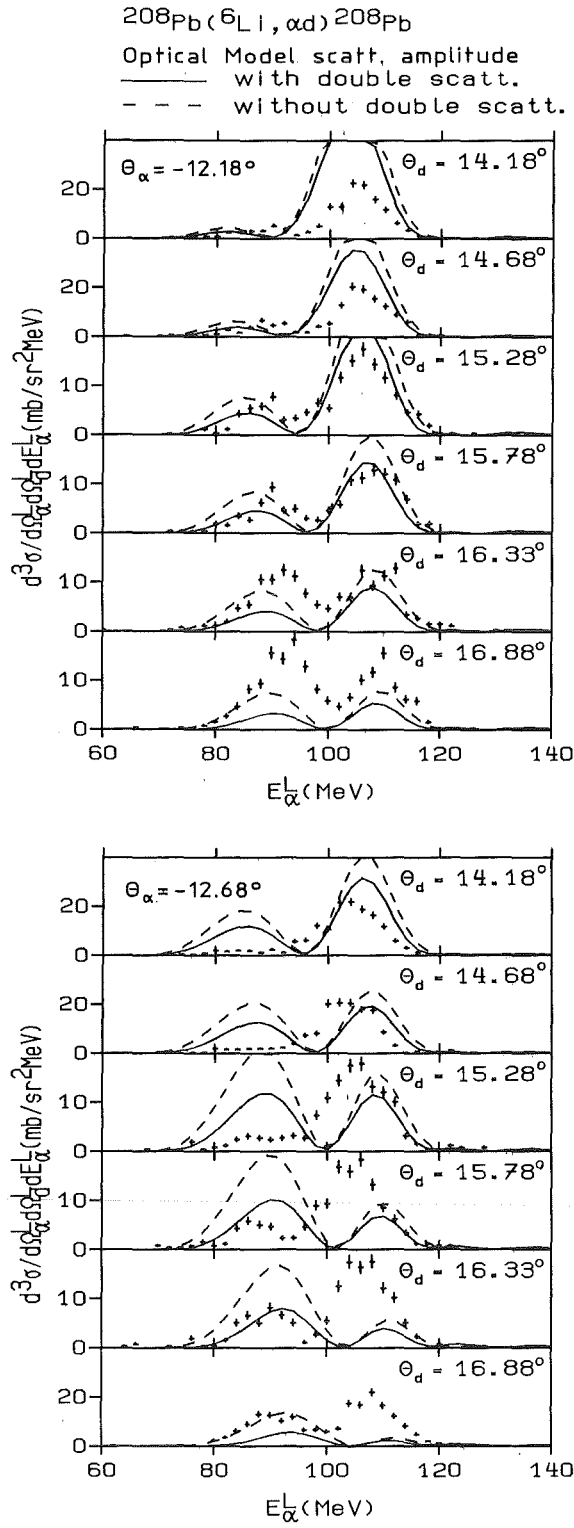
Fig. 14   Experimental and theoretical triple differential cross sections of elastic
break-up of 156 MeV ^{6}Li projectiles colliding with ^{208}Pb: The theoretical
description uses the "optical model" scattering amplitude.

Fig. 15 gives an example where the theoretical cross section is decomposed in the contributions of the α-particle and deuteron interactions. It is also obvious that the contribution of the double-scattering term of eq. (4.7) is generally non negligible, though a definite conclusion about its real significance cannot be drawn. The results demonstrate that the diffraction dissociation approach is able to provide a qualitative understanding of the observed features. However, the present formulation is far from being a quantitative description of the measured cross sections.

$$^{208}Pb(^6Li, \alpha d)^{208}Pb$$
$$\theta_\alpha = -12.18°$$
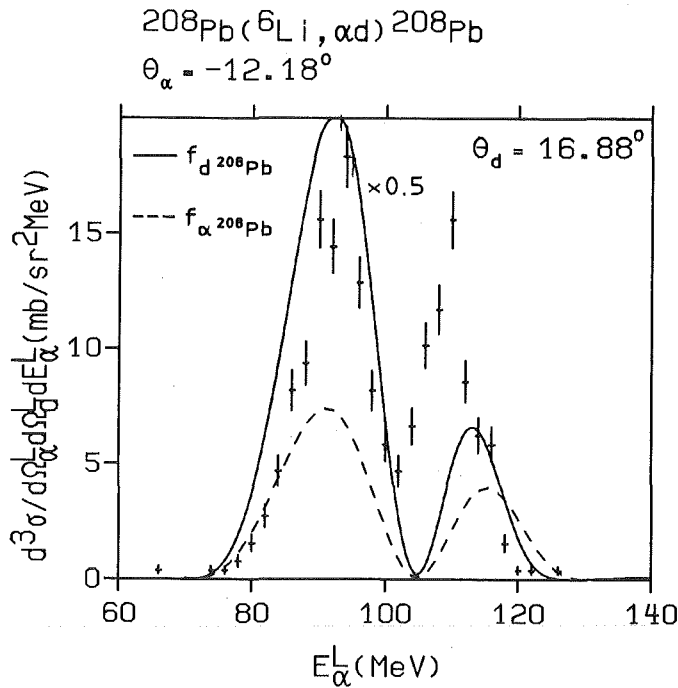
Fig. 15 Contributions from α-particle-target and d-target interactions to the triple differential cross section for break-up of 156 MeV ^{6}Li.

One important deficiency of the present formulation of the diffractive disintegration approach is the restriction to a Yukawa-type 1S ^{6}Li-wave function (eqs. 4.11 - 4.13) which certainly differs from the realistic α - d wave function in the considered range of internal momenta of ^{6}Li. Neglecting the final state interaction we have compared the theoretical predictions based on 1S Yukawa wave function and the 2S wave function proposed by Kukulin et al [13]. The steeper slope and the minimum of the momentum distribution of the 2S function is

clearly reflected by additional structure in the shape and by the magnitude of the cross sections, but does not generally improve the agreement with the experiment. However the effect is considerable and worth considering in further systematic studies including consistently the final state interaction by a more detailed theoretical analysis [18].

5. CONCLUDING REMARKS

The present experiments measuring triple differential cross sections for direct elastic break-up of 156 MeV ^{6}Li projectiles with large relative fragment momenta revealed an unfamiliar type of energy distributions of the correlated break-up α-particles and deuterons. The features, sensitively varying with the relative emission angle i.e. with the total momentum transfer, are basically understood within the framework of the diffractive dissociation approach[6,7], though a quantitative agreement between theoretical predictions and experimental observations is not satisfactorily reached. Various sensitivities to the ingredients of the theory are studied and require a more detailed analysis by an DWBA break-up approach [18] e.g.

REFERENCES

1. R. Serber, Phys. Rev. **72** (1947) 1008

2. R.J. de Meijer and R. Kamermans, Rev. Mod. Phys. **57** (1983) 147

3. R.J. Glauber, Phys. Rev. **99** (1955) 1515

4. H. Rebel, in "Nuclear Collective Dynamics" Lect. at the Int. Summer School of Nucl. Physics, Poiana, Brasov, Romania, 26.8. - 7.9.1982 eds. D. Bucurescu and N.F. Zamfir, World Scientific Publ. Singapore (1983)

5. N. Heide, D.K. Srivastava and H. Rebel, Phys. Rev. Lett. (submitted)

6. A.G. Sitenko, M.V. Evlanov, A.D. Polozov and A.M. Sokolov, Sov. J. Nucl. Phys. **45** (1987) 1320
   A.T. Akhiezer and A.G. Sitenko, Phys. Rev. **106** (1951) 1236

7.   M.V. Evlanov and A.M. Sokolov, Sov. J. Nucl. Phys. 44 (1986) 1191,
     Nucl. Phys. **A452** (1986) 477

8.   H.P. Ehret, R. Ernst, L. Friedrich, A. Hurst, E. Huttel, J. Kaltenbach,
     F. Schulz, L. Wiss and P. Ziegler, KfK-Report 4159, p. 94 eds. G. Büche,
     P. Doll, L. Friedrich, Kernforschungszentrum Karlsruhe 1986

9.   J. Wentz, Diploma Thesis (1989), Universitty of Karlsruhe

10. N. Heide, Internal Report, Kernforschungszentrum Karlsruhe 1988,
     unpublished

11. N. Heide, KfK Report 4551 (1989)

12. G. Baur and D. Trautmann, Phys. Rep. C25 1976) 213
     G. Baur, F. Rösel, D. Trautmann and R. Shyam, ibid C111 (1984) 333

13. V.I. Kukulin, V.M. Krasnopol'ski, V.T. Voronchev, P.B. Sazonov,
     Nucl. Phys. **A417** (1984) 128

14. H. Jelitto, J. Buschmann, V. Corcalciuc, H.J. Gils, N. Heide, J. Kiener,
     H. Rebel, C. Samanta and S. Zagromski
     Z. Phys. **A332** (1989) 317 - KfK-Report 4480 (1988)

15. N. Heide, H. Rebel, V. Corcalciuc and D.K. Srivastava
     Rev. Roum. Phys. (in press)

16. C.A. Bertulani and G. Baur, Nucl. Phys. **A480** (1988) 615

17. J. Cook, H.J. Gils, H. Rebel, Z. Majka and H. Klewe-Nebenius,
     Nucl. Phys. **A388** (1982) 173

18. D.K. Srivastava, H. Rebel and N. Heide (to be published)
     - KfK - Report 4565

APPENDIX

Numerical tables of experimental cross sections for elastic break-up

of 156 MeV ^{6}Li projectiles

Coincidence cross-sections for the direct elastic reaction

$^{208}Pb(^6Li,\alpha d)^{208}Pb$ at 156 MeV.

$\theta_\alpha = \quad -12.18^\circ$

$\theta_d = \quad +16.88^\circ \quad +16.33^\circ \quad +15.78^\circ \quad +15.28^\circ \quad +14.68^\circ \quad +14.18^\circ$

E_α MeV	$d^3\sigma/(d\Omega_\alpha d\Omega_d dE_\alpha)$ mb/$(sr^2 MeV)$					
52	0.39	-.-	0.39	-.-	-.-	-.-
60	-.-	0.39	-.-	-.-	-.-	-.-
64	-.-	-.-	-.-	-.-	0.39	-.-
66	0.39	-.-	-.-	-.-	-.-	-.-
70	-.-	-.-	-.-	-.-	0.39	-.-
72	-.-	0.39	0.39	-.-	0.78	-.-
74	0.39	0.78	0.39	-.-	0.39	-.-
76	0.39	-.-	0.39	-.-	0.39	1.17
78	0.78	1.17	0.39	1.17	0.78	0.78
80	1.56	1.17	1.95	0.39	1.17	0.78
82	2.73	1.95	1.56	1.17	2.73	2.34
84	4.67	4.67	3.51	4.29	1.56	2.34
86	8.18	5.45	2.73	5.45	3.90	3.12
88	9.35	10.52	6.23	5.84	6.62	3.12
90	15.58	10.52	9.35	7.79	4.67	5.06
92	14.41	12.47	4.67	3.12	5.45	3.90
94	18.31	11.30	5.06	3.51	1.95	1.56
96	12.86	7.79	3.12	4.67	1.95	2.73
98	8.18	5.45	2.73	6.62	4.29	5.06
100	5.84	4.67	4.67	5.45	5.45	12.86
102	4.67	7.01	5.84	11.69	12.86	12.86
104	6.62	7.01	10.91	15.19	20.65	22.60
106	10.13	12.47	11.30	17.53	19.48	21.82
108	11.69	9.35	12.86	14.41	15.58	15.97
110	15.58	11.30	12.08	11.69	12.47	11.69
112	8.57	12.86	10.91	8.18	8.96	6.23
114	6.23	3.51	7.01	4.67	6.23	3.51
116	5.84	2.73	1.95	4.29	0.78	1.17
118	1.56	1.56	1.95	1.95	-.-	0.78
120	0.39	1.56	-.-	0.39	0.78	-.-
122	0.39	1.17	-.-	0.39	-.-	-.-
126	0.39	-.-	-.-	0.39	-.-	0.39
130	-.-	0.39	-.-	-.-	-.-	-.-

Coincidence cross-sections for the direct elastic reaction
^{208}Pb(^{6}Li,αd)^{208}Pb at 156 MeV.

θ_d = -14.88°

θ_α = $+16.88^{\circ}$ $+16.33^{\circ}$ $+15.78^{\circ}$ $+15.28^{\circ}$ $+14.68^{\circ}$ $+14.18^{\circ}$

E_α MeV	$d^3\sigma/(d\Omega_\alpha d\Omega_d dE_\alpha)$ mb/(sr^{2}MeV)					
54	0.39	-.-	-.-	-.-	-.-	-.-
60	-.-	-.-	-.-	0.39	0.39	-.-
62	0.78	-.-	-.-	-.-	-.-	0.39
64	0.39	0.39	0.39	-.-	-.-	0.39
66	0.78	0.39	0.39	0.39	0.39	0.78
68	-.-	0.78	1.56	0.39	1.56	0.39
70	0.39	-.-	-.-	0.39	-.-	0.39
72	0.39	0.39	0.39	0.78	0.39	0.78
74	-.-	-.-	0.39	-.-	-.-	0.39
76	-.-	-.-	-.-	-.-	-.-	1.17
78	0.39	-.-	0.39	0.78	-.-	0.39
80	0.78	1.56	0.39	0.39	0.39	0.78
82	0.39	0.78	0.39	2.73	0.39	0.39
84	1.56	1.56	2.34	1.95	2.73	-.-
86	0.39	1.56	2.34	4.67	6.62	1.17
88	0.78	1.95	3.12	3.90	5.84	6.23
90	0.39	-.-	1.17	8.96	9.74	10.91
92	1.95	0.78	2.34	7.01	12.86	13.64
94	6.23	2.34	1.95	5.45	8.57	12.08
96	8.96	7.01	5.45	2.73	8.57	15.58
98	21.04	12.86	6.62	1.17	6.23	12.08
100	19.48	14.80	8.57	3.90	4.67	6.62
102	14.02	21.82	14.80	10.13	5.06	3.12
104	15.97	17.14	18.70	11.69	6.62	3.12
106	10.13	14.02	14.80	14.41	8.18	4.29
108	6.23	12.86	10.91	14.02	8.57	3.12
110	3.51	2.34	10.91	8.18	7.79	6.62
112	1.17	3.90	5.06	6.23	7.40	8.96
114	0.39	-.-	0.39	4.67	4.29	4.29
116	-.-	0.39	0.39	0.78	5.06	1.95
118	0.78	0.39	-.-	0.78	-.-	0.78
120	1.56	-.-	-.-	0.39	1.17	1.17
122	0.78	0.39	0.39	-.-	-.-	0.39
124	0.39	-.-	0.39	-.-	-.-	-.-
126	-.-	-.-	0.39	-.-	-.-	0.39
128	-.-	-.-	-.-	0.78	-.-	-.-
130	-.-	-.-	-.-	0.39	-.-	-.-

Coincidence cross-sections for the direct elastic reaction
$^{12}C(^6Li,\alpha d)^{12}C$ at 156 MeV.

θ_d = -14.88°

θ_α = $+18.88^{\circ}$ $+18.33^{\circ}$ $+17.78^{\circ}$ $+17.28^{\circ}$ $+16.68^{\circ}$ $+16.18^{\circ}$

E_α MeV	$d^3\sigma/(d\Omega_\alpha d\Omega_d dE_\alpha)$ $mb/(sr^2 MeV)$
52	-.-	0.11	0.11	-.-	0.22	-.-
54	0.11	0.11	0.11	0.22	-.-	-.-
56	0.34	0.11	0.11	0.11	0.22	-.-
58	0.22	0.11	0.22	0.45	0.11	-.-
60	0.22	0.22	0.22	0.45	0.22	-.-
62	0.11	0.22	0.22	0.67	0.22	0.34
64	0.34	0.34	0.56	0.78	0.22	0.11
66	0.45	0.56	0.56	0.78	0.22	0.34
68	0.11	0.56	0.56	0.67	0.56	0.11
70	0.34	0.34	0.45	0.90	0.67	0.11
72	1.01	1.34	0.67	0.45	0.22	0.67
74	0.90	0.90	1.23	1.68	0.22	0.11
76	0.56	1.23	1.45	1.01	0.78	0.56
78	0.56	1.45	0.67	2.01	0.67	0.67
80	0.67	1.57	1.34	1.68	1.23	0.56
82	0.90	1.34	1.45	2.24	1.68	2.01
84	0.90	0.56	1.68	1.34	1.12	0.78
86	0.78	0.78	1.90	1.79	1.90	2.35
88	0.56	0.67	1.57	1.90	1.90	1.90
90	0.45	1.12	1.90	1.90	2.01	2.13
92	0.45	0.56	1.45	2.13	2.13	2.24
94	0.34	1.01	2.01	2.13	2.91	3.69
96	0.34	1.45	1.34	2.69	2.69	3.80
98	0.34	0.67	1.90	1.90	1.45	3.13
100	0.56	1.45	1.01	2.80	2.46	4.25
102	0.78	0.67	2.24	2.80	2.69	2.69
104	1.34	1.57	1.01	1.57	2.91	2.69
106	1.57	1.01	1.12	0.67	2.24	2.46
108	1.23	1.23	0.34	1.57	1.90	2.13
110	1.01	0.56	1.12	0.90	0.22	1.79
112	0.78	0.78	0.67	0.90	1.01	0.90
114	0.34	0.22	0.67	1.01	0.67	1.34
116	0.22	0.34	0.11	0.56	0.34	1.23
118	0.45	0.34	0.45	0.22	0.22	0.34
120	0.11	-.-	0.11	-.-	0.22	0.11
122	0.11	-.-	-.-	0.11	-.-	-.-
124	-.-	-.-	0.11	-.-	-.-	-.-
126	-.-	0.11	-.-	0.11	-.-	0.11
128	-.-	0.11	-.-	0.22	-.-	-.-
130	-.-	-.-	-.-	0.11	-.-	-.-
134	0.11	-.-	-.-	-.-	-.-	0.11
136	-.-	-.-	-.-	-.-	0.11	-.-